# Infrared photometry of Young Massive Clusters in the starburst galaxy NGC 4214$^\star$

A. Sollima$^{1,2}$†, R. G. Gratton$^1$, E. Carretta$^2$, A. Bragaglia$^2$, S. Lucatello$^1$

$^1$ *INAF Osservatorio Astronomico di Padova, vicolo dell'Osservatorio 5, Padova, 35122, Italy*
$^2$ *INAF Osservatorio Astronomico di Bologna, via Ranzani 1, Bologna, 40127, Italy*

2 November 2021

**ABSTRACT**

We present the results of an infrared photometric survey performed with NICS@TNG in the nearby starburst galaxy NGC 4214. We derived accurate integrated JK magnitudes of 10 young massive clusters and compared them with the already available Hubble Space Telescope ultraviolet colors. These clusters are located in the combined ultraviolet-infrared colors planes on well defined sequences, whose shapes allow a precise determination of their age. By means of the comparison with suitable stellar evolution models we estimated ages, metallicities, reddening and masses of these clusters. All the analyzed clusters appear to be younger than $\log t/yr < 8.4$, moderately metal-rich and slightly less massive than present-day Galactic globular clusters. The derived ages for clusters belonging to the secondary HII star forming complex are significantly larger than those previously estimated in the literature. We also discuss the possibility of using the ultraviolet-infrared color-color diagram to select candidate young massive clusters hosting multiple stellar populations.

**Key words:** methods: data analysis – methods: observational – techniques: photometric – galaxies: individual: NGC 4214 – galaxies: star clusters: general – infrared: general.

## 1 INTRODUCTION

NGC 4214 is a nearby dwarf IAB(s)m galaxy (de Vaucouleurs et al. 1991) in the low-redshift CVn I Cloud (Sandage & Bedke 1994) located at a distance of $3.04 \pm 0.05$ Mpc (Dalcanton et al. 2009). It has a mass similar to that of the Large Magellanic Cloud (LMC; $M = 5 \times 10^9$ $M_\odot$; Karachentsev et al. 2004) and a moderately low metal-content ($-1.6 < [M/H] < 0$; Williams et al. 2011 hereafter W11). NGC 4214 is characterized by an intense recent star-formation activity, as shown by the presence of two HII star forming complexes located in its central region where several Young Massive Clusters (YMCs) are evident as H$\alpha$ emitting peaks (Fanelli et al. 1997). The young stellar population is embedded in a smooth disk of old stars which account for a significant fraction (up to $\sim 75\%$) of the total stellar mass (W11).

MacKenty et al. (2000) provided a detailed classification

of the H$\alpha$ knots visible in Hubble Space Telescope (HST) images, identifying 13 relatively bright YMCs (see also Fig. 1). The largest star forming complex is located in the northwestern region of NGC 4214 (referred as 4214-I). It is formed by a number of star clusters and has a complex H$\alpha$ structure dominated by the presence of two cavities. Its ultraviolet flux is dominated by an extended YMC (I-As) extending for $\sim$ 70 pc located in a heart-shaped H$\alpha$ cavity. The shell structure of the gas suggests that most of the gas in front of the central star cluster has been removed by the action of stellar winds and supernovae (see also Maíz-Apellániz et al. 1998). The other cavity is occupied by a scaled OB association (I-B) which, at odds with the central cluster, does not show a marked central concentration. Other four knots (I-C, I-Ds, I-Es and I-F) have been identified, probably associated to small associations. In the second complex (4214-II) there is no dominant star cluster but five smaller OB associations (II-A, II-B, II-C, II-D and II-E), responsible for the ionization of the gas, have been detected. In this region there is no clear evidence of decoupling between gas and stars. Both complexes present similar metallicities ($[M/H] \sim$-0.5; Kobulnicky & Skillman 1996) with little dispersion. Other two clusters (IIs and IVs) are present outside the two main complexes, both characterized by a weak H$\alpha$ emission and redder colors. Dust absorption appears to be on average rel-

atively low $(E(B-V) < 0.1)$ although patchy with some regions heavily obscured (Maíz-Apellániz 1998; Drozdovsky et al. 2002; Calzetti et al. 2004; Úbeda, Maíz-Apellániz & MacKenty 2007a; hereafter U07a).

While the diffuse stellar population of NGC 4214 has been the subject of many recent works (Drozdovsky et al. 2002; W11), the study of the star cluster system of NGC 4214 has been restricted to the integrated properties of the two main complexes (Leitherer et al. 1996; Mas-Hesse & Kunth 1999; Hermelo et al. 2012). Recently Úbeda et al. (2007a,b) performed an accurate study using WFPC2@HST observations associated to 2MASS infrared photometry to determine ages, masses, radii and extinction of 11 YMCs. The stellar extinction they estimated appears to follow a Magellanic Cloud-like law and has been found to be quite patchy, with some heavily obscured areas, in particular those associated with star-forming regions. The clusters in complex I and II have been estimated to be very young $(\log t/yr < 7)$ while clusters IIIs and IVs show significantly older ages $(\log t/yr \sim 8)$.

The study of the stellar population of YMCs has deep relevance in the light of the scenario of formation of multiple stellar populations in globular clusters. In fact, in the last decade a growing body of evidence showed that many Galactic globular clusters contain multiple stellar populations which have been evidenced as multiple sequences in various regions of the color-magnitude diagram (e.g. Piotto 2009) and/or as distinct groups of stars with peculiar chemical abundances (Gratton, Carretta & Bragaglia 2012). The above evidence suggests that the stellar populations of these objects are the result of a process of self-enrichment where a second generation of stars formed from the ejecta of a first generation. The observed pattern of abundance variations (light elements anticorrelations with almost constant Fe abundance; Carretta et al. 2009a,b,c) indicates that the responsibles of the chemical pollution must be massive $(M > 5\ M_{\odot})$ stars undergoing high-temperature p-capture nuclear reactions but not supernovae (Langer, Hoffman & Sneden 1993). As a consequence, the entire process of chemical enrichment must have taken place within the first $10^8$ yr i.e. the timescale of evolution of such massive stars (see e.g. D'Antona & Ventura 2007; Decressin et al. 2007 for two possible alternative hypotheses on the nature of the polluters). To date, the phenomenon of multiple populations has been observed in almost all the analyzed globular clusters (with masses $M > 10^5 M_{\odot}$), but not in less massive systems like e.g. open clusters (de Silva et al. 2009; Bragaglia et al. 2012; Geisler et al. 2012). This seems to indicate that the process of formation of multiple populations could start only in systems above a critical mass, able to retain the gas expelled by the early generation of massive stars (Carretta et al. 2010; Bekki 2011). YMCs represent therefore a particularly favorable class of objects to study this phenomenon (see also Peacock, Zempf & Finzell 2013). While resolved photometry is becoming feasible for YMCs in nearby galaxies (Perina et al. 2010; Larsen et al. 2011) the large majority of YMCs are located in distant galaxies where only their integrated properties can be studied.

In this paper we present infrared JK photometry of 10 YMCs of NGC 4214 obtained using NICS@TNG. These data together with the ultraviolet/optical HST photometry of Úbeda et al. (2007b; hereafter U07b) are used to improve the
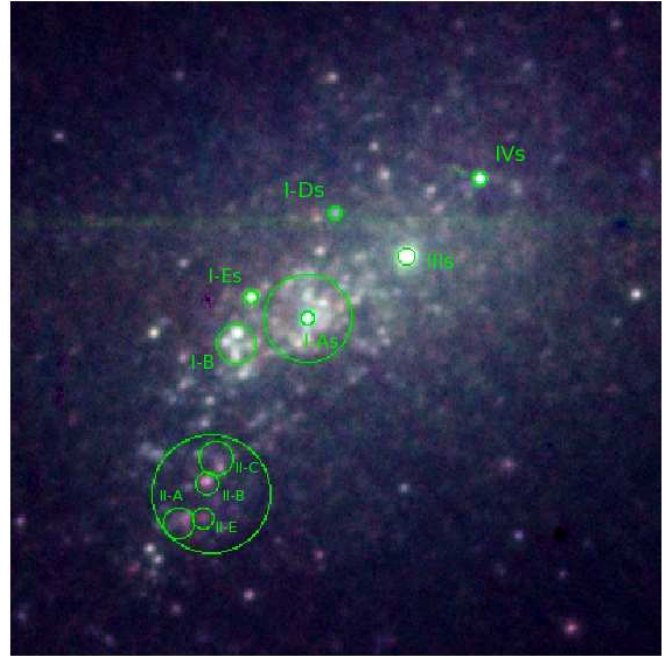


**Figure 1.** Zoomed false-color image of NGC 4214 made using our NICS data. The J,H and K images have been combined in the blue, green and red channels, respectively (in the printed version of the paper the K band image is shown in greyscale). North is up, east to the left. The adopted circular apertures are shown with green circles. The field dimensions are $1.4' \times 1.4'$.

ages, metallicities, masses and reddening determinations of these YMCs. The paper is organized as follow: in Sect. 2 we describe the observations and the data reduction technique. Sect. 3 is devoted to the analysis of the location of YMCs in the ultraviolet-infrared colors planes and the comparison with model predictions. In Sect. 4 the method to derive ages, metallicities and reddening is outlined and the results presented. In Sect. 5 the potential application to multiple stellar populations studies is discussed. Finally, we summarize and discuss our results in Sect. 6.

## 2   OBSERVATIONS AND DATA REDUCTION

Observations were performed during one night on April 11th 2012 at the Telescopio Nazionale Galileo (TNG; Roche de los Muchachos, Spain), equipped with the Near Infrared Camera Spectrometer (NICS). Observations were performed in Service Mode using the large field camera providing a field of view of $4.2' \times 4.2'$ with a pixel scale of $0.25''/px$. The seeing conditions were stable during observations with a $FWHM \sim 1.0''$. A set of 9 images with exposure time $3 \times 20s$ $(NDIT \times DIT)$ has been taken through the J filter and 15 images with exposure time $1 \times 60s$ through the K one, all centered on NGC 4214. Images in the H band were also observed but their signal-to-noise ratios were significantly lower than those in the J and K bands and were not used in the analysis. Science fields have been observed alternately with sky fields (at $\sim 12$ arcmin away from the science field center in a square pattern with the same exposure times of science fields). A median sky image was obtained for each filter and subtracted to science frames. A set of high-S/N

**Table 1.** JK magnitudes of YMCs in NGC 4214.

| cluster | RA (J2000) deg | Dec (J2000) deg | r ″ | J | $\sigma_J$ | K | $\sigma_K$ |
|---|---|---|---|---|---|---|---|
| I-As | 183.9147500 | 36.3268028 | 1.00 | 15.889 | 0.016 | 15.673 | 0.026 |
| I-A | 183.9147083 | 36.3269444 | 6.83 | 13.775 | 0.030 | 13.120 | 0.026 |
| I-B | 183.9183333 | 36.3258833 | 2.96 | 14.896 | 0.008 | 14.129 | 0.018 |
| I-Ds | 183.9134167 | 36.3313778 | 1.00 | 17.400 | 0.017 | 17.128 | 0.053 |
| I-Es | 183.9177500 | 36.3277611 | 1.00 | 16.708 | 0.023 | 15.881 | 0.018 |
| II-A | 183.9216667 | 36.3180889 | 2.28 | 16.424 | 0.014 | 15.538 | 0.029 |
| II-B | 183.9198750 | 36.3197389 | 1.68 | 16.783 | 0.017 | 15.631 | 0.010 |
| II-C | 183.9196667 | 36.3208639 | 2.59 | 16.604 | 0.019 | 15.773 | 0.033 |
| II-E | 183.9202917 | 36.3179750 | 1.59 | 17.549 | 0.020 | 16.497 | 0.035 |
| II | 183.9199583 | 36.3192389 | 9.10 | 14.382 | 0.036 | 13.505 | 0.022 |
| IIIs | 183.9094583 | 36.3295250 | 1.20 | 14.962 | 0.013 | 14.231 | 0.014 |
| IVs | 183.9055833 | 36.3328333 | 1.00 | 16.427 | 0.014 | 15.893 | 0.024 |

flat fields in each filter has been obtained with a halogen lamp and has been used to correct sky-subtracted frames.

We used the aperture photometry algorithm PHOT of the DAOPHOT II package (Stetson 1987) to obtain instrumental magnitudes for all the 10 YMCs detected in each frame (I-As, I-B, I-Ds, I-Es, II-A, II-B, II-C, II-E, IIIs, IVs). The photometry has been performed independently on each frame and calibrated to the 2MASS photometric system using four bright stars present in the field of view of our science frame. The final magnitudes have been obtained as the average of single exposure measures and the related r.m.s. has been assigned as their error. We converted positions from the detector reference frame to celestial coordinates using ∼100 stars well distributed over the NICS field of view and present in the 2MASS catalog. The accuracy of the astrometric solution turns out to be ∼ 0.2″. We adopted the same apertures defined by U07b for most clusters, with the exceptions of clusters I-As, I-Ds, I-Es and IVs: for these objects the apertures defined by U07b are smaller than the resolution of our data, so we adopted in these cases an aperture radius of 1″ (see Fig. 1). For this reason, near infrared JK and HST magnitudes do not contain the same fraction of the cluster flux and therefore cannot be directly compared. The same considerations can be made for the other clusters: as the spatial resolution of our J and K images is significantly worse than that of HST observations, a small but significant part of the cluster light could be spread out the adopted aperture in infrared bands. Thus, only the J-K colors (virtually independent on the aperture size) have been used in the present analysis. As in U07b, two large apertures have been also adopted to measure the integrated magnitudes of the two main star forming complexes (IA and II). The obtained JK magnitudes are listed in Table 1.

The derived JK magnitudes have been complemented with the ultraviolet-optical magnitudes obtained by U07b using the WFPC2 onboard HST. We adopted the magnitudes listed in their Table 6 and 7 which, beside the basic data reduction steps, account for an aperture correction to link the flux measured within the aperture to that at infinity.

## 3 THE ULTRAVIOLET-INFRARED COLOR-COLOR DIAGRAMS

In Fig. 2 the location of the observed clusters in the $(F170W - F336W)vs.(J - K)$ and $(F336W - F555W)vs.(J - K)$ color-color diagrams is shown. It can be noted that in both diagrams the YMCs of NGC 4214 align along well defined, non-monotonic relations: as the ultraviolet colors get redder the J-K color spans a wide range with a first increase (up to $J - K \sim 1.2$ at $F336W - F555W \sim -0.8$), a subsequent blue shift ($J - K \sim 0.5$ at $F336W - F555W \sim -0.2$) and a final reddening. The theoretical evolution in these planes of a young cluster adopting two different metallicities ($[M/H] = -0.5, 0$; appropriated for the recent star formation episodes of a dwarf galaxy such as NGC 4214; W11) are overplotted in both diagrams. These predictions have been obtained by integrating the fluxes predicted by a set of Marigo et al. (2008) isochrones adopting the Kroupa (2001) mass function. We note that, while models fail to reproduce the precise extent of the clusters distribution in the ultraviolet-infrared color-color diagrams, they qualitatively predict their characteristic S-shapes. In fact, stellar population models indicate that during the early evolution of a single stellar population, while ultraviolet colors (dominated by the contribution of Main Sequence stars) become steadily redder, infrared colors are characterized by an initial shift toward the red (after $\sim 6\ 10^6\ yr$ due to the formation of a significant number of Red Supergiants) and a subsequent turnover at $10^8\ yr$ (when the onset of He burning moves stars less massive than $8 - 9\ M_\odot$ toward blue colors). At ages larger than $10^8$ yr the infrared colors become again redder due to the onset of the extended Asymptotic Giant Branch (AGB) phase in stars with masses $M < 5\ M_\odot$. The narrow sequence defined by our data in these planes suggests a rather homogeneous metallicity and reddening distribution across the galaxy. The peculiar shape of the ultraviolet-infrared color-color diagrams allows a very precise determination of clusters ages which is less dependent on the temperature-colors conversion uncertainties than analyses based on optical colors alone (e.g. Fall, Chandar & Whitmore 2005). Indeed, as the infrared color turnovers correspond to phase transitions occurring during the evolution of massive stars, it is possible to infer ages according to the relative position of clusters with respect to
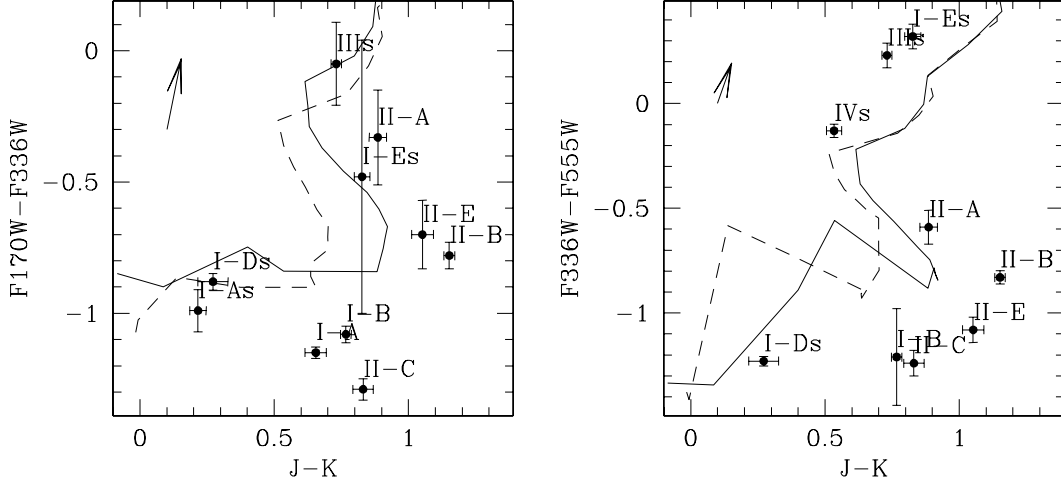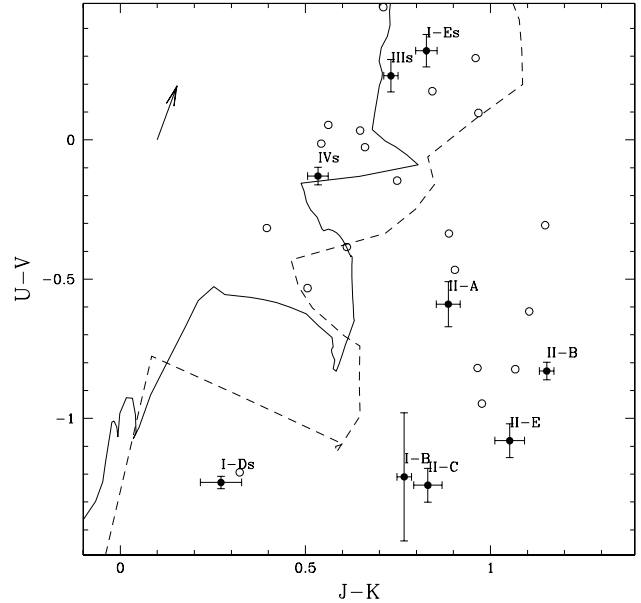
**Figure 2.** Position of the YMCs of NGC 4214 in the $(F170W - F336W)$ *vs.* $(J - K)$ (left panel) and $(F336W - F555W) vs. (J - K)$ (right panel) color-color diagrams. The reddening vectors for E(B-V)=0.1 are shown. Evolutionary models corresponding to metallicities $[M/H] = -0.5$ (dashed lines) and $[M/H] = 0$ (solid lines) are overplotted in both panels.

the *observed* position of such turnovers. The potential power of infrared colors in determining ages of young clusters has been also recently reported by Gazak et al. (2012) who applied a similar technique to a sample of young clusters in M83. Optical colors are less efficient in this regard since they are sensitive to both Main Sequence and evolved stars producing colors always monotonically correlated between them.

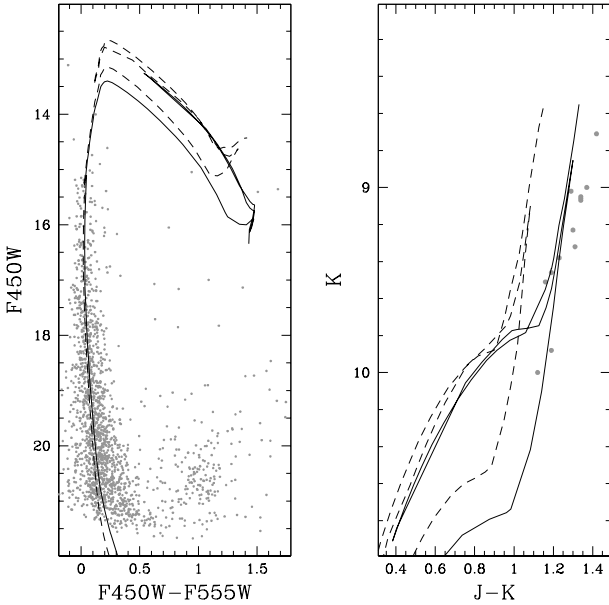### 3.1 Comparison with LMC clusters and theoretical models

As outlined in Sect. 1, NGC 4214 and the LMC share many similarities: they have the same morphological type, similar masses and metal content and both possess a significant population of YMCs. It is therefore interesting to compare the location of their YMCs in the ultraviolet-infrared color-color plane. This is shown in Fig. 3 where the U-V (fairly similar to the $F336W - F555W$ color) and J-K colors for LMC clusters were taken from Searle, Wilkinson & Bagnuolo (1980) and Kyeong et al. (2003), respectively. It is evident that LMC clusters nicely follow the sequence defined by those in NGC 4214, although with a larger scatter.

In both cases stellar populations models provide a poor representation of the data, predicting a significantly less pronounced red excursion at $U - V \sim -0.8$ during the Red Supergiants phase. The same effect is evident adopting different stellar population synthesis models (like Bruzual & Charlot 2003[1]; see Fig. 3). While errors on the photometric calibration and small number fluctuations can con-



**Figure 3.** Position in the $(U - V)$ *vs.* $(J - K)$ color-color diagram of the YMCs of NGC 4214 (filled circles) and of the LMC (from Searle et al. 1980 and Kyeong et al. 2003; open circles). The reddening vector for E(B-V)=0.1 is shown. The evolutionary tracks corresponding to a metallicity $[M/H] = -0.5$ adopting the stellar population synthesis procedure described in this paper (dashed line) and the Bruzual & Charlot (2003) models (solid line) are overplotted.

[1] Both the models adopted in the present work and those by Bruzual & Charlot (2003) make use of the isochrone set by the Padova group. A similar discrepancy is also found using other popular models (see Vázquez & Leitherer 2005).

tribute to such a discrepancy, its presence in both galaxies suggests a problem in the model predictions. The reason of the inadequacy of models can be found by comparing the adopted isochrones with the resolved photometric

crepancy between models and observations, the addition of the IR dimension in the parameter space is still valuable.
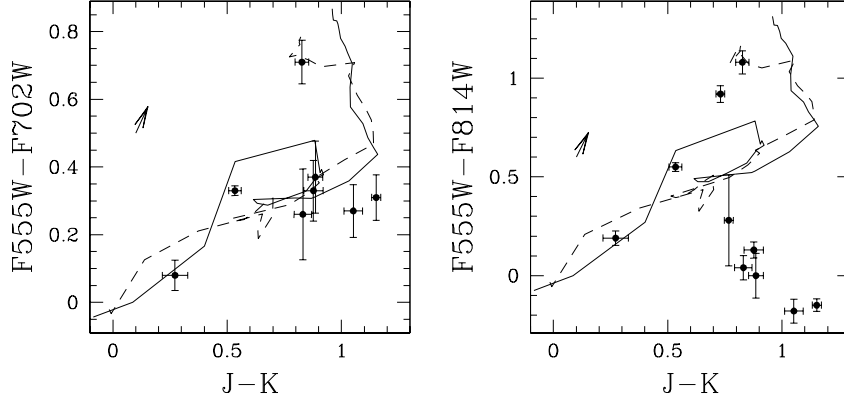
# 4    AGE DETERMINATION

The accurate JK magnitudes, together with the ultraviolet/optical ones measured by U07b, have been used to derive the ages (t), metallicities ($[M/H]$), reddening ($E(B - V)$) and masses (M) of the 10 observed YMCs using a $\chi^2$ minimization technique. As outlined in Sect. 2, because of the different spatial resolution between infrared data and HST observations, the apertures adopted to derive JK magnitudes could contain a different fraction of the cluster flux with respect to HST observations. In this situation, our JK and HST magnitudes cannot be used together to search for the best model. On the other hand, in absence of color gradients, the J-K color should be independent on the aperture size within the region dominated by the cluster. So, we calculated the $\chi^2$ comparing each HST magnitude and the J-K color with models (avoiding the individual use of J and K magnitudes). To check the dependence of the obtained results on this last choice, we repeated the analysis considering J and K magnitudes separately (instead of the J-K color alone): for clusters with the same aperture the results remain unchanged (within $\Delta \log t/yr < 0.1$) and found a discrepancy which grows almost linearly with the difference of aperture to a maximum of $\Delta \log t/yr \sim 0.3$. So the above described effect is small while still present. Consider that even for those clusters for whom we adopted the same aperture of U07a we cannot assume that HST and IR magnitudes contain the same fraction of the cluster flux. For this reason we prefer to leave the J-K color as a single independent constraint.

For each cluster, we searched the best combination of the above parameters that minimize the penalty function[2]

$$\chi^2 = \sum_{i=1}^{N} \frac{(M_i^{mod} + DM + E(B - V) \, k_i - 2.5 \, \log M - m_i^{obs})^2}{\sigma(m_i)^2 + \epsilon^2} + \frac{((J - K)^{mod} - (J - K)^{obs})^2}{\sigma(J - K)^2 + 2 \, \epsilon^2} \quad (1)$$

where $m_i^{obs}$ and $M_i^{mod}$ are the i-th magnitude and the prediction of the stellar population model for 1 $M_\odot$ at a given metallicity and age, $\sigma(m_i)$ is the error on the magnitude $m_i^{obs}$, $DM = 27.41$ is the distance modulus of NGC 4214 (Dalcanton et al. 2009), $k_i = A_\lambda/E(B - V)$ is the reddening coefficient in the i-th band (from Girardi et al. 2008, Marigo et al. 2008), $\log M$ is the logarithm of the cluster mass, $N$ is the number of adopted magnitudes and $\epsilon$ is a softening parameter (set to 0.05 mag in all filters; see Whitmore et al. 2010) which accounts for the models errors. Note that the logarithm of the cluster mass is included in eq. 1 as a constant term to be subtracted to each magnitude. So, while ages and metallicities are determined only by colors, masses are determined from the scaling factor providing the bestfit



**Figure 4.** $F450W - (F450W - F555W)$ (from Brocato et al. 2001; left panel) and $K - (J - K)$ (from Keller 1999; right panel) CMDs of NGC 2100. The isochrones corresponding to a metallicity $[M/H] = -0.5$ (dashed line) and $[M/H] = 0$ (solid lines) are overplotted in both panels.

data available for some LMC cluster populating this region of the $U - V \, vs. (J - K)$ color-color diagram. In Fig. 4 the $F450W - (F450W - F555W)$ (from Brocato, Di Carlo & Menna 2001) and $K - (J - K)$ (from Keller 1999) color-magnitude diagrams (CMDs) of the cluster NGC 2100 (having integrated colors $U - V = -0.4$ and $J - K = 1.19$) are compared with the same isochrones of the Marigo et al. (2008) set used to compute the stellar population evolutionary sequences in Fig. 2 (with metallicity $[M/H] = -0.5$ and $[M/H] = 0$, bracketing the metallicity estimates for this cluster by Jasniewicz & Thevenin 1994, Hill & Spite 1999 and Colucci et al. 2011). Adopting a distance modulus of $(m - M)_0 = 18.50$ (Sebo et al. 2002) the bestfit age and reddening for this cluster turn out to be $\log t/yr = 7.35$ and $E(B - V) = 0.3$, almost independent on the adopted metallicity. The isochrones, while fitting well the optical CMD, are some 0.1-0.3 mag bluer than the observed stars in the infrared CMD. Such a difference can account entirely for the J-K color difference between models and observations in Figs. 2 and 3 and is probably linked to the uncertainties in the color-temperature transformations for the cold ($T \sim 3500 \, K$) Red Supergiants which dominate the infrared luminosity.

However, although stellar evolution models do not provide an optimal representation of the data in the age interval $6.8 < \log t/yr < 8$ (where most of the considered clusters lie), they qualitatively predict the shift toward red colors observed in both NGC 4214 and LMC YMCs. This allows to identify those clusters in the relatively fast stage in which Red Supergiants dominate their infrared flux, whose ages could not be unambiguously determined using ultraviolet/optical colors alone. So, in spite of the apparent dis-

---

[2] The formalism of eq. 1 is equivalent to consider all the linearly independent colors composed by the HST magnitudes and the J-K color to estimate ages, metallicities and reddenings.

**Figure 5.** Position of the YMCs of NGC 4214 in the $(F555W - F702W)$ *vs.* $(J - K)$ (left panel) and $(F555W - F814W) vs. (J - K)$ (right panel) color-color diagrams. The reddening vectors for E(B-V)=0.1 are shown. Evolutionary models corresponding to metallicities $[M/H] = -0.5$ (dashed lines) and $[M/H] = 0$ (solid lines) are overplotted in both panels.
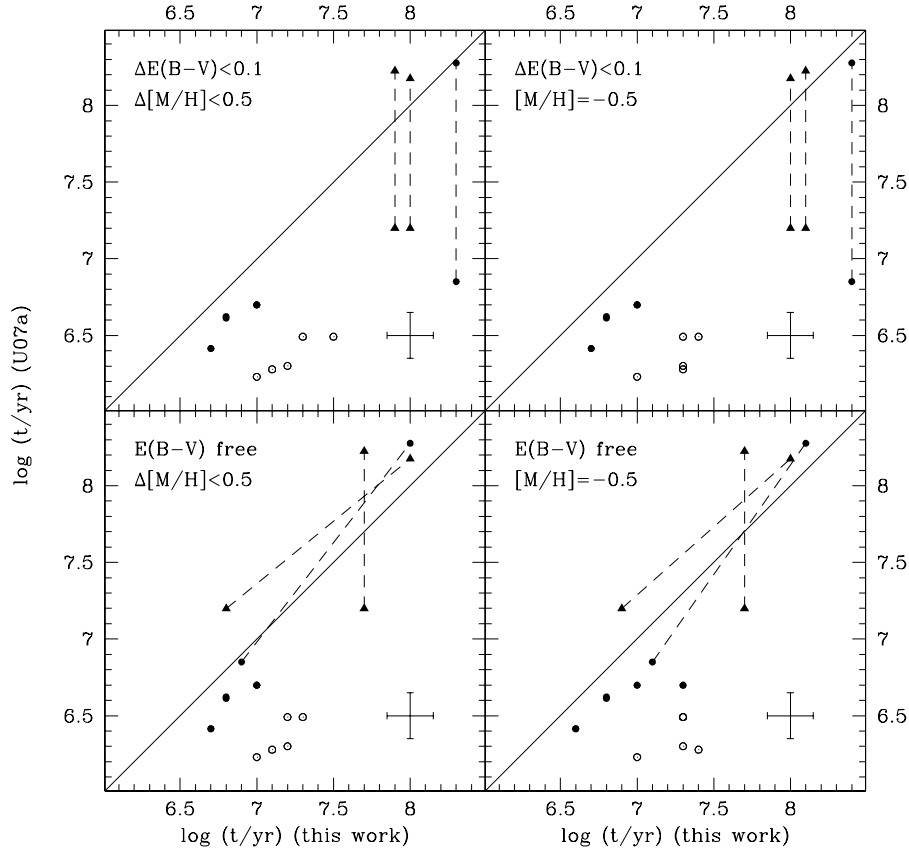


**Figure 6.** Comparison between the ages estimated in this work and in U07a. In the bottom panels the comparison is made with ages derived leaving the reddening as a free parameter, while in the upper panels ages derived constraining the reddening to span a $\Delta E(B - V) < 0.1$ range are considered. In the left panels the comparison is made with ages derived constraining the metallicity to span a $\Delta [M/H] < 0.5$ range, while in right panels ages derived assuming a fixed metallicity [M/H]=-0.5 are considered. Filled dots indicate clusters belonging to complex I, open dots indicate clusters belonging to complex II, triangles indicates other clusters. The ranges covered by multiple age solutions are indicated by dashed lines. The one-to-one relation is also shown as solid line in all panels. Typical uncertainties are also indicated.

**Table 2.** Derived parameters of YMCs in NGC 4214.

| | Metallicity within $\Delta[M/H] < -0.5$ | | | | | | | | | |
|---|---|---|---|---|---|---|---|---|---|---|
| | Reddening left free | | | | | Reddening within $\Delta E(B-V) < 0.1$ | | | | |
| cluster | $\log t/yr$ | [M/H] | $\log M/M_\odot$ | E(B-V) | $\chi^2/n$ | $\log t/yr$ | [M/H] | $\log M/M_\odot$ | E(B-V) | $\chi^2/n$ |
| I-As | 6.8 | -0.3 | 4.81 | 0.04 | 0.005 | 6.8 | -0.3 | 4.81 | 0.04 | 0.005 |
| | ($\pm$0.1) | ($\pm$0.1) | ($\pm$0.02) | ($\pm$0.01) | | ($\pm$0.1) | ($\pm$0.1) | ($\pm$0.02) | ($\pm$0.01) | |
| I-A | 7.0 | -0.4 | 5.61 | 0.00 | 0.008 | 7.0 | -0.3 | 5.68 | 0.03 | 0.712 |
| | ($\pm$0.1) | ($\pm$0.1) | ($\pm$0.02) | ($\pm$0.01) | | ($\pm$0.1) | ($\pm$0.3) | ($\pm$0.06) | ($\pm$0.01) | |
| I-B | 7.0 | -0.1 | 4.99 | 0.01 | 0.135 | 7.0 | -0.2 | 5.03 | 0.03 | 0.210 |
| | ($\pm$0.2) | ($\pm$0.2) | ($\pm$0.04) | ($\pm$0.02) | | ($\pm$0.1) | ($\pm$0.3) | ($\pm$0.05) | ($\pm$0.01) | |
| I-Ds | 6.7 | 0.0 | 4.15 | 0.13 | 1.199 | 6.7 | 0.0 | 4.15 | 0.13 | 1.199 |
| | ($\pm$0.1) | ($\pm$0.5) | ($\pm$0.12) | ($\pm$0.09) | | ($\pm$0.1) | ($\pm$0.3) | ($\pm$0.12) | ($\pm$0.05) | |
| I-Es | 6.9 | 0.0 | 4.07 | 0.54 | 0.771 | 8.3 | 0.2 | 4.68 | 0.13 | 1.002 |
| | ($\pm$0.1) | ($\pm$0.3) | ($\pm$0.10) | ($\pm$0.12) | | ($\pm$0.2) | ($\pm$0.4) | ($\pm$0.11) | ($\pm$0.05) | |
| " | 8.0 | -0.5 | 4.70 | 0.31 | 0.828 | | | | | |
| | ($\pm$0.4) | ($\pm$0.3) | ($\pm$0.08) | ($\pm$0.07) | | | | | | |
| II-A | 7.2 | -0.2 | 5.17 | 0.25 | 0.013 | 7.5 | 0.2 | 5.21 | 0.13 | 0.101 |
| | ($\pm$0.2) | ($\pm$0.1) | ($\pm$0.07) | ($\pm$0.05) | | ($\pm$0.1) | ($\pm$0.3) | ($\pm$0.03) | ($\pm$0.02) | |
| II-B | 7.2 | 0.0 | 4.80 | 0.09 | 2.852 | 7.2 | 0.0 | 4.80 | 0.09 | 2.852 |
| | ($\pm$0.3) | ($\pm$0.3) | ($\pm$0.15) | ($\pm$0.06) | | ($\pm$0.3) | ($\pm$0.3) | ($\pm$0.15) | ($\pm$0.05) | |
| II-C | 7.0 | -0.2 | 4.61 | 0.00 | 2.800 | 7.0 | -0.3 | 4.66 | 0.03 | 5.437 |
| | ($\pm$0.1) | ($\pm$0.3) | ($\pm$0.21) | ($\pm$0.01) | | ($\pm$0.2) | ($\pm$0.5) | ($\pm$0.35) | ($\pm$0.01) | |
| II-E | 7.3 | 0.0 | 4.53 | 0.03 | 1.762 | 7.3 | 0.1 | 4.52 | 0.03 | 1.757 |
| | ($\pm$0.3) | ($\pm$0.3) | ($\pm$0.17) | ($\pm$0.05) | | ($\pm$0.3) | ($\pm$0.3) | ($\pm$0.11) | ($\pm$0.03) | |
| II | 7.1 | 0.0 | 5.52 | 0.01 | 2.599 | 7.1 | 0.0 | 5.56 | 0.03 | 2.893 |
| | ($\pm$0.3) | ($\pm$0.5) | ($\pm$0.39) | ($\pm$0.03) | | ($\pm$0.3) | ($\pm$0.3) | ($\pm$0.22) | ($\pm$0.02) | |
| IIIs | 7.7 | -0.2 | 5.23 | 0.24 | 0.001 | 7.9 | 0.2 | 5.23 | 0.13 | 0.010 |
| | ($\pm$0.1) | ($\pm$0.1) | ($\pm$0.03) | ($\pm$0.01) | | ($\pm$0.1) | ($\pm$0.1) | ($\pm$0.15) | ($\pm$0.01) | |
| IVs | 6.8 | -0.1 | 4.56 | 0.46 | 0.002 | 8.0 | -0.3 | 5.13 | 0.13 | 0.217 |
| | ($\pm$0.1) | ($\pm$0.1) | ($\pm$0.05) | ($\pm$0.03) | | ($\pm$0.1) | ($\pm$0.2) | ($\pm$0.06) | ($\pm$0.01) | |
| " | 8.0 | -0.5 | 5.13 | 0.15 | 0.006 | | | | | |
| | ($\pm$0.1) | ($\pm$0.1) | ($\pm$0.01) | ($\pm$0.01) | | | | | | |

magnitudes. As the apertures adopted for some clusters in the J and K images differ from those defined by U07b (see Sect. 2), we have not used them to constrain cluster masses. Errors have been calculated estimating the parameter interval where the probability associated to the $\chi^2$ include 68% of the probability integrated over the entire parameter range[3] In our procedure we adopted only the F170W, F336W and F555W magnitudes derived by U07b, excluding the F702W and F814W ones. In fact, these magnitudes have only a poor discriminating power and for many clusters observations significantly deviate from the model predictions by several times the nominal uncertainties. This is shown in Fig. 5 where the $J-K$ *vs.* $F555W - F702W$ and the $J-K$ *vs.* $F555W - F814W$ color-color diagrams are shown. An age degeneracy is apparent in both planes during the Red Supergiants phase (at $0.5 < J-K < 1$) which is noticeable as a closed loop in these diagrams. Furthermore, the observed F555W-F814W colors stray from the model prediction by several times their formal error, indicating a possible inadequacy of models and/or photometric calibration. It is worth noting that the apparent discrepancy between models and observations reported in the previous section could

[3] Note that the errors do not depend on the absolute value of the $\chi^2$ but on its variation across the parameter space. For this reason a few clusters with relatively large values of $\chi^2/n$ (possibly due to model inadequaces; see Sect. 3.1) in Table 2 can have small errors in the derived parameters.

in principle affect age determinations. In this regard, when the clusters' colors are driven by the contribution of Main Sequence stars (at ages $\log t/yr < 6.8$ and $\log t/yr > 8$; see Fig. 9b) clusters follow a monotonic ultraviolet-infrared color-color relation which is well reproduced by models. On the other hand, in the age interval $7 < \log t/yr < 7.5$ J-K colors are dominated by Red Supergiants and are expected to exhibit a significant infrared excess which can be easily identified by the $\chi^2$ minimization technique described above even if the value of the J-K color is not exactly predicted by models. The inadequacy of the models could instead affect age determinations for clusters in the age interval immediately before ($6.8 < \log t/yr < 7$) and after ($7.5 < \log t/yr < 8$) the maximum red shift, when the contribution of Main Sequence and Red Supergiants balance between them. The ages of these clusters depend on the relative contribution of Main Sequence and Red Supergiants which is not correctly reproduced by theoretical models. As a consequence, for these clusters an intermediate age could be erroneously assigned. These age ranges are however relatively short and only few clusters are expected to be affected by this uncertainty.

In principle, all parameters can be allowed to vary across the parameter space. However, to limit the degeneracy of our solutions we considered two cases: *i)* constrain cluster-to-cluster metallicitiy variations to lie within a range of $\Delta[M/H] = 0.5$ *dex* around a mean value, and *ii)* keep metallicity fixed to the spectroscopic measure by Kobul-

**Table 2.** Derived parameters of YMCs in NGC 4214. (continued)

| | Metallicity fixed to [M/H]=-0.5 | | | | | | | | | |
| | Reddening left free | | | | | Reddening within $\Delta E(B-V) < 0.1$ | | | | |
| cluster | $\log t/yr$ | [M/H] | $\log M/M_\odot$ | E(B-V) | $\chi^2/n$ | $\log t/yr$ | [M/H] | $\log M/M_\odot$ | E(B-V) | $\chi^2/n$ |
|---|---|---|---|---|---|---|---|---|---|---|
| I-As | 6.8 | -0.5 | 4.89 | 0.07 | 0.558 | 6.8 | -0.5 | 4.89 | 0.07 | 0.558 |
|  | ($\pm$0.1) | | ($\pm$0.08) | ($\pm$0.03) | | ($\pm$0.1) | | ($\pm$0.06) | ($\pm$0.03) | |
| I-A | 7.0 | -0.5 | 5.62 | 0.01 | 0.121 | 7.0 | -0.5 | 5.66 | 0.03 | 0.363 |
|  | ($\pm$0.1) | | ($\pm$0.02) | ($\pm$0.01) | | ($\pm$0.1) | | ($\pm$0.06) | ($\pm$0.01) | |
| I-B | 7.3 | -0.5 | 5.23 | 0.00 | 1.071 | 7.0 | -0.5 | 5.01 | 0.04 | 1.157 |
|  | ($\pm$0.3) | | ($\pm$0.14) | ($\pm$0.02) | | ($\pm$0.1) | | ($\pm$0.05) | ($\pm$0.01) | |
| I-Ds | 6.6 | -0.5 | 4.17 | 0.18 | 1.899 | 6.7 | -0.5 | 4.13 | 0.13 | 3.679 |
|  | ($\pm$0.1) | | ($\pm$0.13) | ($\pm$0.08) | | ($\pm$0.1) | | ($\pm$0.12) | ($\pm$0.05) | |
| I-Es | 7.1 | -0.5 | 4.55 | 0.68 | 2.129 | 8.4 | -0.5 | 4.63 | 0.13 | 1.189 |
|  | ($\pm$0.2) | | ($\pm$0.28) | ($\pm$0.14) | | ($\pm$0.2) | | ($\pm$0.12) | ($\pm$0.06) | |
| " | 8.1 | -0.5 | 4.70 | 0.31 | 0.904 | | | | | |
|  | ($\pm$0.4) | | ($\pm$0.08) | ($\pm$0.07) | | | | | | |
| II-A | 7.3 | -0.5 | 5.22 | 0.24 | 0.631 | 7.4 | -0.5 | 5.10 | 0.13 | 1.880 |
|  | ($\pm$0.2) | | ($\pm$0.08) | ($\pm$0.06) | | ($\pm$0.1) | | ($\pm$0.024) | ($\pm$0.03) | |
| II-B | 7.3 | -0.5 | 4.86 | 0.10 | 9.544 | 7.3 | -0.5 | 4.86 | 0.10 | 9.544 |
|  | ($\pm$0.3) | | ($\pm$0.16) | ($\pm$0.07) | | ($\pm$0.3) | | ($\pm$0.16) | ($\pm$0.06) | |
| II-C | 7.0 | -0.5 | 4.57 | 0.00 | 3.801 | 7.0 | -0.5 | 4.64 | 0.03 | 5.915 |
|  | ($\pm$0.1) | | ($\pm$0.21) | ($\pm$0.01) | | ($\pm$0.2) | | ($\pm$0.35) | ($\pm$0.01) | |
| II-E | 7.3 | -0.5 | 4.51 | 0.05 | 7.163 | 7.3 | -0.5 | 4.51 | 0.05 | 7.163 |
|  | ($\pm$0.3) | | ($\pm$0.17) | ($\pm$0.05) | | ($\pm$0.3) | | ($\pm$0.17) | ($\pm$0.05) | |
| II | 7.4 | -0.5 | 5.75 | 0.00 | 3.727 | 7.3 | -0.5 | 5.71 | 0.03 | 4.678 |
|  | ($\pm$0.3) | | ($\pm$0.41) | ($\pm$0.04) | | ($\pm$0.3) | | ($\pm$0.23) | ($\pm$0.03) | |
| IIIs | 7.7 | -0.5 | 5.29 | 0.28 | 0.024 | 8.1 | -0.5 | 5.29 | 0.12 | 0.194 |
|  | ($\pm$0.1) | | ($\pm$0.07) | ($\pm$0.04) | | ($\pm$0.2) | | ($\pm$0.16) | ($\pm$0.02) | |
| IVs | 6.9 | -0.5 | 4.61 | 0.41 | 0.006 | 8.0 | -0.5 | 5.11 | 0.13 | 0.189 |
|  | ($\pm$0.1) | | ($\pm$0.06) | ($\pm$0.04) | | ($\pm$0.1) | | ($\pm$0.06) | ($\pm$0.01) | |
| " | 8.0 | -0.5 | 5.13 | 0.15 | 0.010 | | | | | |
|  | ($\pm$0.1) | | ($\pm$0.01) | ($\pm$0.01) | | | | | | |

nicky & Skillman (1996; [M/H]=-0.5). This is an appropriate choice as it is not plausible that a larger chemical enrichment could occur in the recent star formation history of this galaxy (see also W11). Reddening can instead vary across the field of view by several magnitudes being very patchy (U07a). Leaving reddening as a free parameter has however the drawback of favoring the well known age-reddening degeneracy, i.e. old clusters with intrinsically red colors can be also identified as young clusters with a high degree of reddening. In fact, following this approach two clusters have two solutions with similar likelihood (clusters I-Es and IVs) appearing very young and obscured ($\log t/yr < 7$; $E(B - V) > 0.4$) when reddening is left as a free parameter, while they result significantly older ($\log t/yr > 8$) when adopting a small extinction value. So, we also performed our analysis constraining the reddening to vary from cluster-to-cluster within a range of $\Delta E(B - V) = 0.1$ around a mean value. The mean values of metallicity and reddening have been chosen as those that minimize the sum of the $\chi^2$ of the 10 clusters. In Table 2 the results of our analysis are listed for all the above described assumptions on metallicity and reddening. We note that all the approaches lead to very similar estimated ages. The differences between the solutions obtained with the two assumptions on metallicity are consistent within $\Delta \log t/yr < 0.3$. When the reddening is constrained to vary by only a small amount the two clusters with multiple solutions (I-Es and IVs) appears both relatively old ($\log t/yr > 8$). The lack of a significantly intense

$H\alpha$ emission in the direction of these clusters (MacKenty et al. 2000) favors this last hypothesis.

In Fig.s 6 and 7 the ages and masses of the 10 YMCs derived in this paper are compared with those estimated by U07a. For a few clusters (IEs, IIIs and IVs in U07a; IEs and IVs in our analysis conducted leaving reddening as a free parameter) two independent solutions with young and old ages are provided. In these cases the comparison has been made between the pair of young and old solutions obtained by both works. It is immediately evident that while the ages we derived for clusters belonging to the star forming complex I agree within the errors with those estimated by U07a, our ages are on average larger for all clusters belonging to the star forming complex II. Some differences between the analysis performed here and that by U07a could play a role: the adopted stellar models, the different resolution of the two datasets, etc. However, the main reason for the different age estimates stands in the different choice of the filters for the $\chi^2$ minimization algorithm. In particular, in our work the J-K color accounts for a significant fraction of the entire likelihood. Instead, in U07a only few clusters (none of them belonging to complex II) have available infrared magnitudes. Moreover, the large errors associated to the 2MASS magnitudes give negligible weights to infrared colors and the age determination is driven by the ultraviolet-optical properties of the clusters. So, the large J-K excess visible in Fig. 2 is interpreted in our analysis as the effect of a significant
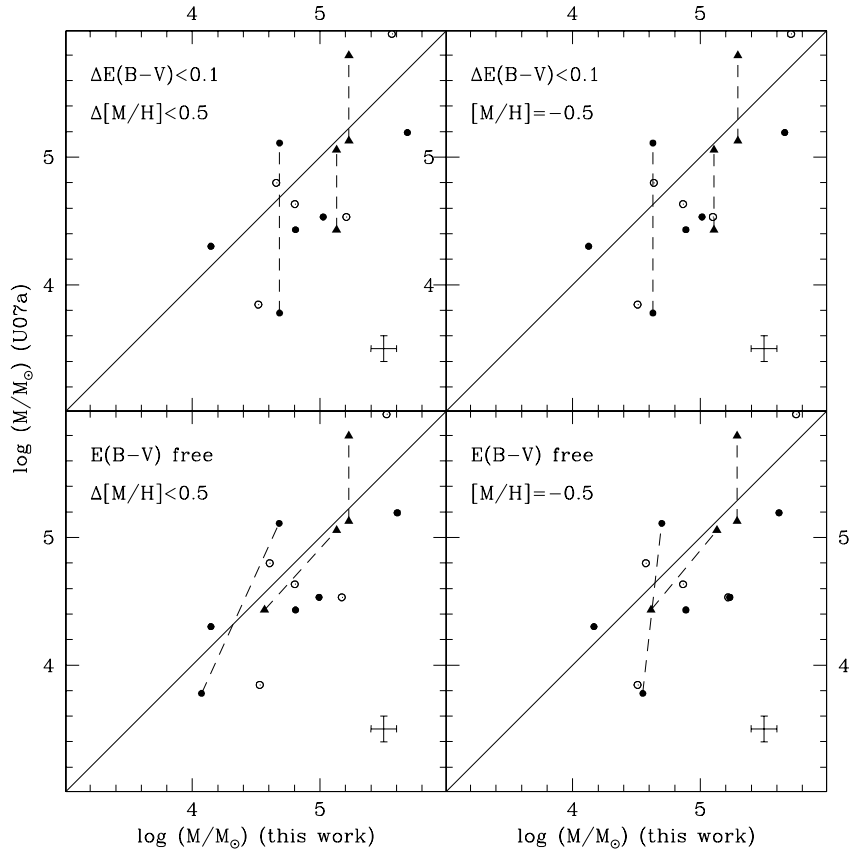
**Figure 7.** Comparison between the masses estimated in this work and in U07a. Symbols and lines are as in Fig. 6.
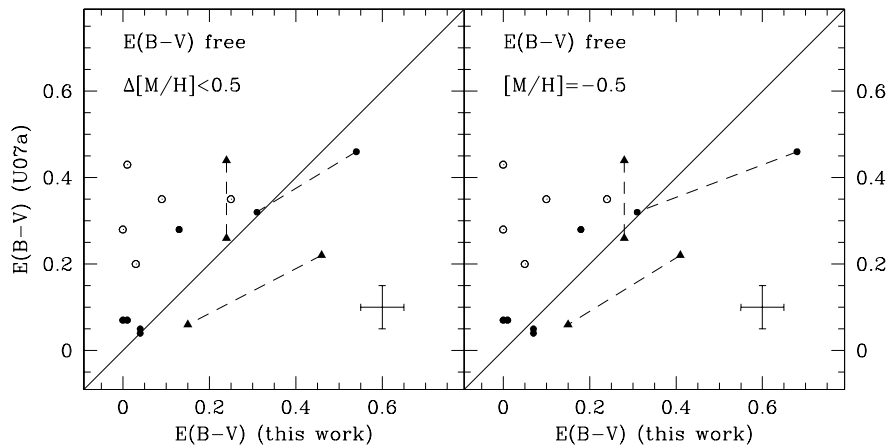


**Figure 8.** Comparison between the reddening estimated in this work and in U07a. Symbols and lines are as in Fig. 6.

contribution of Red Supergiants which are effective after $\sim 6 \ 10^6 \ yr$ at $[M/H] \sim 0$.

In Fig. 8 the reddening estimates are compared. Of course, a meaningful comparison is possible only for the estimates made without any prior. Also in this case, the reddening estimated for clusters belonging to complex I agree

within the errors with those provided by U07a, while for clusters in complex II our estimates are significantly smaller. This is also a consequence of the age-reddening degeneracy: to reproduce optical colors (which come from the same analysis of U07a) the effect on colors produced by the older ages

we derived for these clusters is compensated by a smaller reddening.

Masses appears instead only slightly larger than those listed by U07a. This is an implicit consequence of the above discussed age difference: since the mass-to-light ratios of old clusters are larger than those of young ones, the same luminosity is interpreted as a larger mass in the former case. Reddening differences play also a role: in clusters where significantly smaller reddenings have been estimated (see above), the effect on magnitudes is compensated by a slightly smaller mass.

# 5    THE ULTRAVIOLET-INFRARED PLANE AS A TOOL TO IDENTIFY MULTIPLE-POPULATIONS IN YMCS?

The peculiar shape of the ultraviolet-infrared color-color diagram shown in Fig. 2 can in principle represent an useful tool to select good candidates to host multiple populations. Indeed, the combination of two stellar populations with similar metallicities and different ages would produce a cluster with a color

$$A - B = (A_f - B_f) - 2.5 \, log \left( \frac{1 - \eta + \eta \; 10^{0.4(A_f - A_s)}}{1 - \eta + \eta \; 10^{0.4(B_f - B_s)}} \right)$$

where A-B is an arbitrary color, $\eta$ is the relative mass fraction of the second generation and the subscripts refer to first ($f$) and second ($s$) generations. In Fig. 9a the location in the ($F170W - F336W$) $vs.$ ($J - K$) color-color diagram of a cluster formed by two generations of stars with ages $log \, t/yr$=7.6 and 6.8 ($\Delta t \sim 30 \; Myr$), [M/H]=0 and different population ratios $\eta$ is compared with the track of single population clusters with the same metallicity. It is evident that multiple populations clusters with $0.1 < \eta < 0.5$ occupy a region forbidden to single population clusters. The identification of some cluster in this region could therefore indicate the presence of multiple populations. In panel b the same diagram is shown considering different ages for the second generation (adopting always an age difference between the two populations of $\Delta t \sim 30 \; Myr$; the minimum evolutionary timescale for a massive AGB star; D'Antona & Ventura 2008). It is evident that clusters cross the forbidden region only if the second generation is younger than $log \, t/yr < 7$. Finally, in panel c the same diagram is shown assuming a lower metallicity [M/H] = −1.0. In this case, the extent of the red excursion due to the Red Supergiants is significantly reduced (because of ombined effect of the higher temperature of the Hayashi track and of the shorter time spent in the Red Supergiants phase) and the forbidden region almost disappears. A very similar conclusion has been reached by Peacock et al. (2013) who however consider optical colors instead of infrared ones. As shown in Sect. 3, infrared colors are more suitable for this purpose, maximizing the extent of the turnover thus allowing a much clear identification of multiple populations clusters.

Unfortunately, many sources of scatter in this diagram complicate the task. First, as discussed above, the position of the multiple population region depends on metallicity. The above method works only when relatively high ([M/H] > −0.5) and homogeneous metallicities are involved. This is however the situation for most galaxies,

where the most recent episodes of star formation are characterized by high metal content (Terlevich & Forbes 2002). Second, most YMCs are often embedded in dust-rich clouds with strong absorption up to several visual magnitudes (like in the Antennae galaxies and M83; Mengel et al. 2005; Kim et al. 2012). This has only a minor effect on infrared colors but produces a significant shift in ultraviolet ones. Hence, the location of multiple population clusters can be reached also by young but highly reddened single population clusters. The effects of the above sources of uncertainties can be partly reduced by adopting several combinations of ultraviolet colors which can break the age-metallicity-reddening degeneracy. Third, uncertainties in the calibration and the aperture selection can introduce a spread of several tenths of magnitudes (in particular in small clusters). Fourth, in young clusters integrated fluxes are dominated by red/blue Supergiants which are in fast evolutionary stages. Therefore, only few stars determine the color of a stellar populations and small number fluctuations can introduce significant scatter in the above diagram (see the discussion in Gazak et al. 2012). This last effect can be however negligible if massive ($M > 10^6 M_\odot$) clusters are considered. Fifth, as shown in Sect. 3.1, models often provide a poor representation of the observational data. This can be due for instance to the uncertainties in color-temperature transformation (see Fig. 4) or to the uncertainties in the core/envelope overshooting efficiency which determines the fraction of blue-loop/Red Supergiants stars (McQuinn et al. 2011). In this regard, the agreement between the distribution of clusters in the ($U - V$) $vs.$ ($J - K$) diagram for both NGC 4214 and the LMC (Fig. 3) seems to suggest the possibility of using *empirical* evolutionary sequences to define the locus of single stellar population clusters in these diagrams.

# 6    DISCUSSION AND SUMMARY

In this work we used the infrared JK integrated magnitudes obtained from a dedicated NICS@TNG survey of 10 YMCs in the nearby starburst galaxy NGC 4214 to derive their ages, metallicities, reddening and masses. By combining infrared magnitudes with ultraviolet ones already available from high-resolution HST observations we note that these clusters are located in the combined ultraviolet-infrared color-color planes on well defined sequences, whose shapes allow a precise determination of their age, with a resolution of $\sigma(log \, t/yr) \sim 0.1$. From our analysis all clusters are relatively young ($6.7 < log \, t/yr < 8.3$, with a median value of $log \, t/yr = 7.15$) and metal-rich ($-0.5 < [M/H] < 0$) with masses in the range $4.1 < log \, M/M_\odot < 5.7$. For comparison, the young ($< 1 \; Gyr$) population of clusters of the LMC has an age distribution peaked at a significantly larger age ($log \, t/yr \sim 7.9$; Popescu, Hanson & Elmegreen 2012), as expected given the higher star-formation rate of NGC 4214 with respect to the LMC. While the derived ages of clusters in the 4214-I complex are in good agreement with those estimated by U07a, the clusters in the 4214-II complex appear to be significantly older than what previously estimated. The difference stems from the extremely red J-K color of many clusters, which is interpreted as due to a significant contribution of Red Supergiants (which are effective after $\sim 10^7 \; yr$ at [M/H] $\sim 0$). The detection of a significant
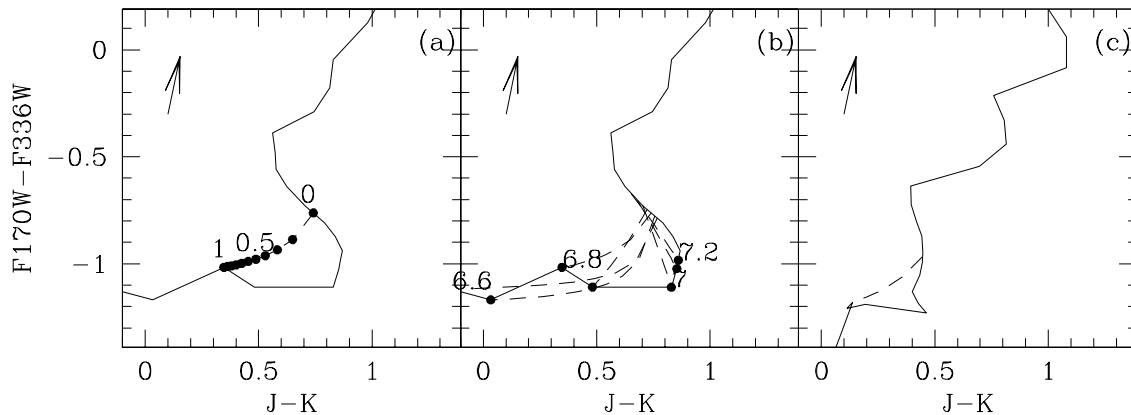
**Figure 9.** Locus of a cluster formed by first/second generations with different second generation mass fractions (dashed lines). In panel (a) the ages $\log t/yr$ =7.6 and 6.8 for the two generations and a metallicity of $[M/H] = 0$ have been adopted. In panel (b) an age differences of $\Delta t = 30 \; Myr$ between the two generations and different ages of the second generation have been adopted. Panel (c) is the same of panel (a) but for a metallicity $[M/H] = -1.0$. Evolutionary tracks of single stellar population clusters (solid lines) and the reddening vector corresponding to E(B-V)=0.1 are shown in all panels.

population of Red Supergiants in these objects through future resolved HST photometry could indicate the veridicity of this last interpretation.

The estimated metallicities are in agreement with that provided by W11 for the young field population of NGC 4214 ($-0.6 < [M/H] < 0$) and are higher than the mean metallicity of the old galactic population ($-1.6 < [M/H] < -0.6$).

It can be noted that even leaving reddening as a free parameter the derived reddening does not exceed $E(B-V) = 0.55$, with a median value of $E(B-V) = 0.065$. On the other hand, if we constrain reddening to lie within a 0.1 range, the bestfit range turns out to be $E(B-V) = 0.08 \pm 0.05$. The above values are compatible with the estimated foreground Galactic reddening by Schlegel, Finkbeiner & Davis (1998). This indicates that, on average, the YMCs of NGC 4214 lie in a relatively optically thin region. Similar conclusions have been reached by Lee et al. (2009) and W11. This also explain the well defined turnover in the ultraviolet-infrared colors.

The masses of these clusters are only slightly smaller than those of present-day Galactic globular clusters. The most massive and compact among these objects will evolve toward a globular cluster-like structure. It is therefore possible to consider these objects as the young counterparts of globulars. Note however that, according to the scenario proposed by D'Ercole et al. (2008), Galactic globular clusters were ∼10 times more massive than the YMCs of NGC 4214. It is therefore unprobable that these clusters will undergo the same chemical evolution of Galactic globular clusters.

We discussed the possibility of using ultraviolet-infrared color-color diagrams to test the presence of multiple populations in YMCs. While we find no evidence of multiple populations in the YMCs of NGC 4214, this tool can be in principle effective in selecting good candidates for clusters characterized by high-metallicity ($[M/H] > -1$), low reddening ($E(B-V) < 0.1$) and a young ($\log t/yr < 7$) sec-

ond generation constituting a cluster mass fraction in the range $0.1 < \eta < 0.5$. Although the above constraints reduce the detection efficiency and the inadequacy of stellar evolution models in infrared bands prevents from any conclusive detection, the ultraviolet-infrared color-color diagrams can be used in statistical sense if many YMCs are observed. Galaxies characterized by a high star formation rate (e.g. starburst galaxies) represent a good benchmark to test this tool providing a large number of YMCs within a relatively chemically homogeneous environment.

## REFERENCES

Bekki K., 2011, MNRAS, 412, 2241
Bragaglia A., Gratton R. G., Carretta E., D'Orazi V., Sneden C., Lucatello S., 2012, A&A, 548, A122
Brocato E., Di Carlo E., Menna G., 2001, A&A, 374, 523
Bruzual G., Charlot S., 2003, MNRAS, 344, 1000
Calzetti D., Harris J., Gallagher J. S., Smith D. A., Conselice C. J., Homeier N., Kewley L., 2004, AJ, 127, 1405
Carretta E., et al., 2009a, A&A, 505, 117

Carretta E., Bragaglia A., Gratton R., Lucatello S., 2009b, A&A, 505, 139

Carretta E., Bragaglia A., Gratton R., D'Orazi V., Lucatello S., 2009c, A&A, 508, 695

Carretta E., Bragaglia A., Gratton R. G., Recio-Blanco A., Lucatello S., Gratton R. G, 2010, A&A, 516, A55

Colucci J. E., Bernstein R. A., Cameron S. A., McWilliam A., 2011, ApJ, 735, 55

Dalcanton J. J., et al., 2009, ApJS, 183, 67

D'Antona F., Ventura P., 2007, MNRAS, 379, 1431

Decressin T., Meynet G., Charbonnel C., Prantzos N., Ekström S., 2007, A&A, 464, 1029

de Silva G. M., Gibson B. K., Lattanzio J., Asplund M., 2009, A&A, 500, L25

de Vaucouleurs G., de Vaucouleurs A., Corwin H. G. Jr., Buta R. J., Paturel G., Fouquè P., 1991, Third Reference Catalogue of Bright Galaxies. Volume I-III, Springer eds., New York, NY (USA)

Drozdovsky I. O., Schulte-Ladbeck R. E., Hopp U., Greggio L., Crone M. M., 2002, AJ, 124, 811

Fall S. M., Chandar R., Whitmore B. C., 2005, ApJL, 631, L133

Fanelli M. N., et al., 1997, ApJ, 481, 735

Gazak J. Z., Bastian N., Kudritzki R. P., Adamo A., Davies B., Plez B., Urbaneja M. A., 2013, MNRAS, 430, L35

Geisler D., Villanova S., Carraro G., Pilachowski C., Cummings J., Johnson C. I., Bresolin F., 2012, ApJ, 756, L40

Girardi L., et al., 2008, PASP, 120, 583

Gratton R. G., Carretta E., Bragaglia A., 2012, A&ARv, 20, 50

Hermelo I., Lisenfeld U., Relaño M., Tuffs R. J., Popescu C. C., Groves B., 2013, A&A, 549, 70

Hill V., Spite M., 1999, Ap&SS, 265, 469

Jasniewicz G., Thevenin F., 1994, A&A, 282, 717

Karachentsev I. D., Karachentseva V. E., Huchtmeier W. K., Makarov D. I., 2004, AJ, 127, 2031

Keller S. C., 1999, AJ, 118, 889

Kim H., et al., 2012, ApJ, 753, 26

Kobulnicky H. A., Skillman E. D., 1996, ApJ, 471, 211

Kroupa P., 2001, MNRAS, 322, 231

Kyeong J.-M., Tseng M.-J., Byun Y.-I., 2003, A&A, 409, 479

Langer G. E., Hoffman R., Sneden C., 1993, PASP, 105, 301

Larsen S. S.,et al., 2011, A&A, 532, A147

Lee J. C., et al., 2009, ApJ, 706, 599

Leitherer C., Vacca W. D., Conti P. S., Filippenko A. V., Robert C., Sargent W. L. W., 1996, ApJ, 465, 717

MacKenty J. W., Maíz-Apellániz J., Pickens C. E., Norman C. A., Walborn N. R., 2000, AJ, 120, 3007

Maíz-Apellániz J., Mas-Hesse J. M., Munoz-Tunon C., Vilchez J. M., Castaneda H. O., 1998, A&A, 329, 409

Marigo P., Girardi L., Bressan A., Groenwegen M. A. T., Silva L., Granato G. L., 2008, A&A, 482, 883

Mas-Hesse J. M., Kunth D., 1999, A&A, 349, 765

McQuinn K. B. W., Skillman E. D., Dalcanton J. J., Dolphin A. E., Holtzman J., Weisz D. R., Williams B. F., 2011, ApJ, 740, 48

Mengel S., Lehnert M. D., Thatte N., Genzel R., 2005, A&A, 443, 41

Peacock M. B., Zepf S. E., Finzell T., 2013, ApJ, in press, arXiv:1304.0477

Perina S., et al., 2010, A&A, 511, A23

Piotto G., 2009, "The Ages of Stars", Proceedings of the International Astronomical Union, IAU Symposium, 258, 233

Popescu B., Hanson M. M., Elmegreen B. G., 2012, ApJ, 751, 122

Sandage A., Bedke J., 1994, The Carnegie Atlas of Galaxies. Volumes I, II., Carnegie Institution of Washington Publ., No. 638

Schlegel D. J., Finkbeiner D. P., Davis M., 1998, ApJ, 500, 525

Searle L., Wilkinson A., Bagnuolo W. G., 1980, ApJ, 239, 803

Sebo K. M., et al., 2002, ApJS, 142, 71

Stetson P. B., 1987, PASP, 99, 191

Terlevich A. I., Forbes D. A., 2002, MNRAS, 330, 547

Úbeda L., Maíz-Apellániz J., MacKenty J. W., 2007b, AJ, 133, 917

Úbeda L., Maíz-Apellániz J., MacKenty J. W., 2007a, AJ, 133, 932

Vázquez G. A., Leitherer C., 2005, ApJ, 621, 695

Whitmore B. C., et al., 2010, AJ, 140, 75

Williams B. F., Dalcanton J. J., Gilbert K. M., Seth A. C., Weisz D. R., Skillman E. D., Dolphin A.E., 2011, ApJ, 735, 22